



# Lawrence Berkeley Laboratory

UNIVERSITY OF CALIFORNIA

RECEIVED

## Materials & Molecular Research Division

AUG 6 1981

DOCUMENTS SECTION

Presented at the Meeting of the Electrochemical Society, Symposium on Electrocatalysis, Minneapolis, MN, May 10-15, 1981; and to be published in the Proceedings

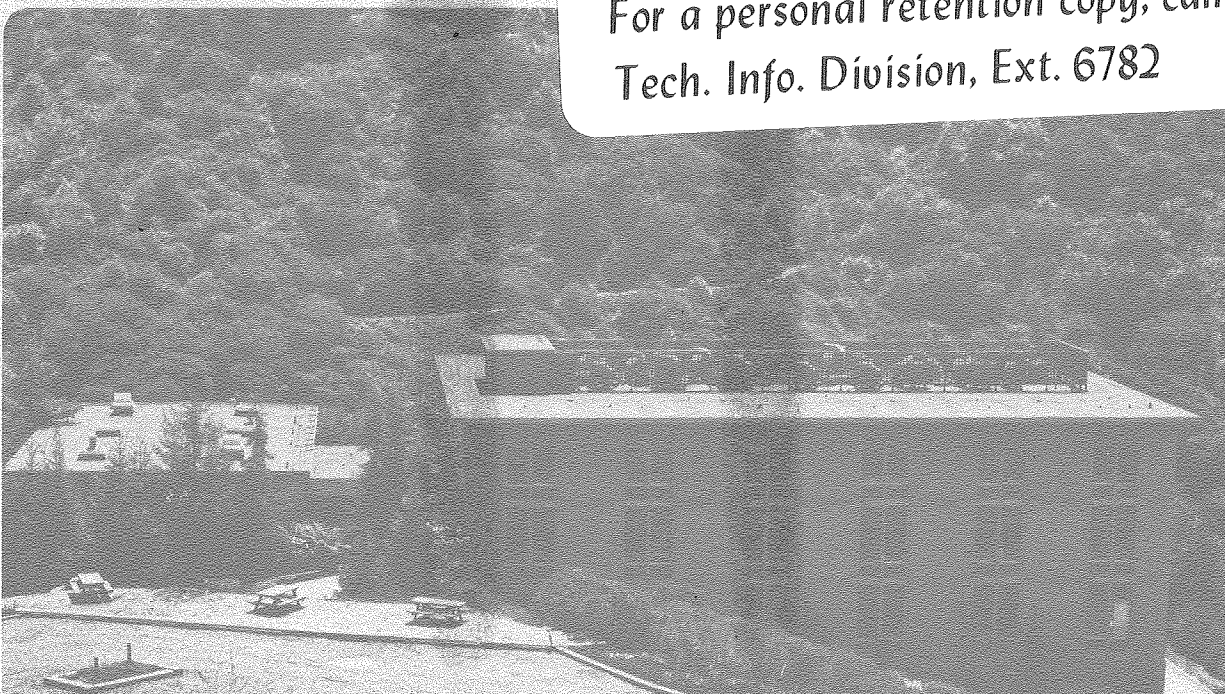
OXYGEN REDUCTION WITH CARBON SUPPORTED METALLIC CLUSTER CATALYSTS IN ALKALINE ELECTROLYTE

Philip N. Ross, Jr.

March 1981

**TWO-WEEK LOAN COPY**

This is a Library Circulating Copy which may be borrowed for two weeks. For a personal retention copy, call Tech. Info. Division, Ext. 6782



LBL-11891

## **DISCLAIMER**

This document was prepared as an account of work sponsored by the United States Government. While this document is believed to contain correct information, neither the United States Government nor any agency thereof, nor the Regents of the University of California, nor any of their employees, makes any warranty, express or implied, or assumes any legal responsibility for the accuracy, completeness, or usefulness of any information, apparatus, product, or process disclosed, or represents that its use would not infringe privately owned rights. Reference herein to any specific commercial product, process, or service by its trade name, trademark, manufacturer, or otherwise, does not necessarily constitute or imply its endorsement, recommendation, or favoring by the United States Government or any agency thereof, or the Regents of the University of California. The views and opinions of authors expressed herein do not necessarily state or reflect those of the United States Government or any agency thereof or the Regents of the University of California.

Oxygen Reduction with Carbon Supported Metallic Cluster Catalysts  
in Alkaline Electrolyte

Philip N. Ross, Jr.

Materials and Molecular Research Division  
Lawrence Berkeley Laboratory  
University of California  
Berkeley, CA 94720

Abstract. The atomic structure of clusters of Pt group metals dispersed on carbon blacks was examined using transmission electron microscopy (TEM) and extended x-ray absorption fine structure (EXAFS) spectroscopy. Both the catalyzation procedure and the microstructure of the carbon influence the resulting structure of the metal cluster. Colloidal catalyzation of Pt onto a turbostratic carbon black support yields a metallic cluster with an amorphous structure, i.e., no atomic order. The amorphous structure is metastable, undergoing an ordering transition at temperatures above ca. 800 C. The amorphous form of Pt interacts with both oxygen and water more strongly than the crystalline form. This stronger interaction produces characteristically different kinetic behavior of the catalysts for oxygen reduction. These differences take the form of a compensation effect, with lower activation energy and lower pre-exponential factor for the amorphous clusters. The properties of highly dispersed Pt clusters relative to the bulk form appears to be a general feature of the Group VIII metals, e.g., Ir, Pd, Rh, and Ru.

## 1. Introduction

In the practical use of electrocatalysts for electrode processes, one usually attempts to obtain the highest possible surface area of the catalytic material to minimize the amount of material. However, for certain catalysts and for some reactions the activity of the catalyst may not be directly proportional to the area. This would be the case for catalysts and/or reactions which are site specific, and the number of active sites does not scale by surface area. Cases of this kind have been termed "demanding" (1) or "structure sensitive" (2) by workers in heterogeneous catalysis, and a good deal more is known about such effects in that field than in electrocatalysis. Probably the best known example of a demanding reaction in electrocatalysis is hydrogen molecule oxidation on tungsten carbide (3), and it seems likely that catalysts of that generic type, i.e., transition metal carbides, would also be site specific. Purely metallic catalysts, particularly the Pt group

This manuscript was printed from originals provided by the author.

metals, represent an entirely different generic class. The preferred embodiment of this type of catalyst, both in hydrocarbon processes and in electrode processes, is as clusters of atoms (microcrystals) dispersed on a support material. The best known example of a supported electrocatalyst is the Pt on carbon black fuel cell catalyst (4). The initial question in the utilization of supported electrocatalysts is whether the catalytic activity per surface atom changes as a function of the state of dispersion of the metal. In spite of the technological importance of this fundamental question, little basic research has been conducted on this subject outside of groups at United Technologies (5). This question has been and remains a primary topic of inquiry in our research group. In particular, we have been studying the effect of the state of dispersion of Pt on the kinetics of reduction of oxygen with supported catalysts. Previous studies of this effect had been contradictory; an accounting of the situation as of 1978 is given in a previous electrocatalysis symposium volume (6). From results obtained in the last three years of study, the effect of the state of dispersion of Pt on the kinetics of oxygen reduction, and the reasons for apparently contradictory observations in acid electrolyte, can be explained (7).

The purpose of the present report is twofold. First, the characterization of the microstructure of Pt clusters is summarized. It is then shown, in summary, how the cluster microstructure affects certain properties of the electrocatalyst in both acid and alkaline electrolyte. Finally, a general extension to the properties of other Group VIII metals when highly dispersed on carbon is suggested.

## 2. Characterization of Pt on Carbon

### 2.1 Microstructure determination

It is possible to distinguish two entirely different types of Pt on carbon catalysts in both microstructure and electrochemical behavior: 1) Pt dispersion on a graphitic carbon black via an ion-exchange catalyzation procedure (8), and 2) Pt dispersed on a turbostratic carbon black via a colloidal (sol) catalyzation procedure (9). The microstructure of the resulting Pt clusters is related both to the microstructure of the carbon and to the catalyzation procedure. In the ion-exchange procedure, the graphitic carbon surface is oxidized with chromic acid to create -COOH acid sites for titration against the Pt salt solution containing  $\text{Pt}(\text{NH}_3)_4(\text{OH})_2$ . Hydrogen reduction following ion exchange causes the formation of single Pt ad-atoms on the carbon surface which rapidly coalesce and grow into clusters. The atomic ordering in these clusters is clearly fcc microcrystalline, as seen by both high-resolution electron microscopy (TEM) and extended x-ray absorption fine structure (EXAFS). A characteristic TEM image is

shown in Fig. 1. The resolved graphite layer plane provides an internal calibration of the dimensionality of the Pt clusters. The image shows beautifully formed hexagonal profile microcrystals with ordered surface facets. The images are consistent with the cubo-octahedral structure expected from thermodynamic calculations (10). The particle size distribution was quite broad, 30-100 Å, but there was no evidence of very small clusters, e.g., <20 Å. Hydrogen and carbon monoxide chemisorption indicated the dispersion (percent of surface atoms) was typically 25-35 percent (a nominal Pt surface area of 70-90 m<sup>2</sup>/g) for this type of catalyst.

The colloidal catalyzation procedure yields a different type of Pt cluster. A hydrated Pt oxide sol is created by reaction of the complex Pt sulfite acid  $\text{H}_3\text{Pt}(\text{SO}_3)\text{OH}$  with  $\text{H}_2\text{O}_2$  (9) and the sol is adsorbed onto the carbon surface. The adsorption onto the carbon appears to occur at Lewis acid sites, as this catalyzation works well only with acidic carbon blacks. Heating the catalyst in hydrogen at 200-300 °C reduces the Pt oxide particles to a metallic (zero-valent) state as confirmed by ESCA. The TEM of Pt dispersed on the furnace black Vulcan XC-72 (Cabot) is shown in Fig. 2. The carbon black has a turbostratic microstructure; the Pt clusters appear to have a spherical profile. Examination of the Pt clusters in an atomic resolution microscope failed to produce any lattice imaging within the clusters of Fig. 2, whereas lattice images (Pt (111) layer planes) were easily obtained for the clusters of Fig. 1, as reported previously by Jalan (11). EXAFS spectra provided definitive evidence for the absence of crystallographic ordering within the Pt clusters of Fig. 2. These spectra are shown in Figs. 3 and 4. The ordinate in these figures is a radial structure function which is proportional to the number of atoms in each coordination shell (see (12) for a review of EXAFS). With a Pt foil in this apparatus, the first four coordination spheres are easily resolved. The peak in the structure function is displaced from the crystallographic radius for each coordination shell by the phase shift (12) which is 0.14 Å in the case of Pt. The EXAFS spectrum for the colloidal Pt on Vulcan catalyst has only one coordination sphere, indicating insufficient ordering occurs beyond nearest neighbors to produce interference in the photoelectron plane-wave. Figure 4 shows the contrast in the structure function for the colloidal Pt on Vulcan and Pt on graphitized Vulcan; in the latter, sufficient ordering exists to cause interference of the photoelectron wave from scattering off second nearest neighbors. The single peak type of structure function is often seen for transition metals close to the melting point (13), and one is tempted to characterize the microstructure in this case as "liquid-like."

In the colloidal catalyzation procedure, the Pt cluster is actually formed in solution at room temperature, then adsorbed as a cluster onto the support. Solution clusters are certain to be amorphous, but the surprising result is that reduction at 200-300 °C does not cause ordering in the clusters. In the ion-exchange

technique, the clusters are grown on the support from individual metal atoms, plus they have an ordered hexagonal surface on which epitaxial nucleation might be expected. When the Vulcan carbon support was catalyzed via the ion-exchange technique, the resulting microstructure of the clusters was essentially the same as for the colloidal catalyst except for a much broader distribution in cluster size, 10 Å - 50 Å. It seems reasonable to conclude that the turbostratic microstructure of the carbon prevents epitaxial growth of clusters from individual atoms. Also, the metal-support interaction may be strong enough to prevent metal-metal ordering in the cluster during hydrogen reduction of clusters on the Vulcan carbon support. Supporting this contention are the remarkable high-resolution TEM images obtained by Jalan (11) showing raft-like shapes for the Pt clusters on Vulcan carbon that might indicate strong metal-support interaction. Heat treating of Pt on Vulcan carbon catalyst in an inert atmosphere required temperatures above 800 C to cause restructuring of the clusters (to an ordered microstructure), which is further evidence that a significant potential well is created by the metal-support interaction. There are, therefore, a number of consistent observations suggesting that both the carbon microstructure and the catalyzation procedure play a role in determining the microstructure of the dispersed Pt phase.

For the purposes of convenience in subsequent discussions, we shall refer to the two extreme cases of Pt microstructure described in the preceding passages as amorphous and microcrystalline. Amorphous refers to that state of Pt produced specifically when Vulcan XC-72 carbon is catalyzed with Pt via the colloidal method. Microcrystalline shall refer to that produced specifically when graphitized Vulcan XC-72 carbon is catalyzed via the ion-exchange technique.

## 2.2 Electrochemical characterization

The underpotential states of hydrogen and oxygen on these supported catalysts are characteristically different. The cyclic current-potential (voltammetry) curves are shown in Figs. 5 and 6. In acid, the underpotential hydrogen peaks are dramatically different for the colloidal Pt on Vulcan catalyst, with the major peak being intermediate between the "weak" and "strong" hydrogen peaks normally seen on polycrystalline Pt. The underpotential states of hydrogen on the microcrystalline Pt with the graphitic carbon support are "normal" in this sense. The unusual states of underpotential hydrogen on highly dispersed Pt had been observed previously by Stonehart and co-workers (15). The explanation advanced in that work was that this unique underpotential state of hydrogen represented adsorption at Pt sites of low coordination number, such as the edges and vertices of microcrystalline particles (16). From the study of the Pt microstructure discussed above, Pt clusters that display this unique state of hydrogen are

not microcrystalline, i.e., they have no well ordered planes or facets from which edge or corner sites are formed. However, the average coordination number for these clusters is lower than the expected value of 9-10, and may be as low as 4-6. It does seem likely that the unique state of hydrogen seen on amorphous Pt clusters is associated with the poorly ordered state and the low coordination number for Pt atoms on the surface of these clusters. The underpotential states of oxygen are also characteristically different between catalysts of differing microstructure. The differences are more subtle than in the case of hydrogen and are not, for example, dramatically evident in a single cyclic voltammetry curve at room temperature, as in Fig. 5. In examining curves at elevated temperatures in  $\text{H}_3\text{PO}_4$ , dramatic differences do appear, and from these one can calculate a difference in adsorption enthalpy for underpotential oxygen from acid solution on amorphous and microcrystalline forms of Pt of ca. 7 kcal/equiv. (two electrons per equiv.), the adsorption being the stronger on the amorphous clusters.

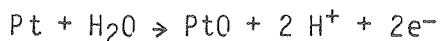
The underpotential deposition of oxygen from alkaline solutions showed (Fig. 6) some features not seen in adsorption from acid solutions. Underpotential deposition of oxygen starts at much lower potentials than in acid, as low as 0.5 V vs RHE. Further, the UPD oxygen is reversible at potentials up to ca. 1.0 V. For polycrystalline Pt, two reversible states are distinguished, at ca. 0.63 V and 0.90 V. At room temperature, the voltammetry curve for amorphous Pt clusters is not dramatically different than for crystalline Pt, but there are three reversible states distinguishable, the new state being at ca. 0.7 V. From variable temperature curves, the enthalpy of UPD oxygen is again found to be higher for the amorphous Pt catalyst—by about 8 kcal/equiv. It is curious that the new state of UPD oxygen occurs at a bond energy intermediate between the "weak" and "strong" states on a polycrystalline Pt surface, as was the case for UPD hydrogen from acid.

The conclusion to be drawn from the electrochemical characterization is that the interaction between amorphous Pt clusters and water is stronger than is the case with microcrystalline or polycrystalline Pt. This stronger interaction causes underpotential deposition of oxygen to occur at more cathodic potentials on the amorphous clusters; likewise, at a fixed potential, the coverage of UPD oxygen will be greater on the amorphous clusters than on the microcrystallites. Also, the amorphous clusters appear to have adsorption sites not found on low-index surfaces.

### 3. Kinetics of Oxygen Reduction

The experimental method for obtaining kinetic data with supported electrocatalyst has been described at length

elsewhere (17). Here we discuss, specifically, the results for the two supported catalysts described above compared to those obtained with a standard smooth Pt rotating disk electrode (RDE). A comparison of the kinetic polarization (corrected for diffusion) behavior of the colloidal Pt on Vulcan catalyst with a smooth Pt RDE is shown in Fig. 7. The activation energy in the 120 mV region was 8.2 kcal/mole for the supported catalyst, 10.5 kcal/mole for smooth Pt. The polarization behavior for the graphite-supported catalyst, and other heat-treated Pt on Vulcan catalysts that were characterized as microcrystalline (17) were observed to be essentially indistinguishable from the smooth Pt RDE. The polarization curve for amorphous Pt was distinguished from all others by (i) a transition in Tafel slope that occurred at more cathodic potentials, (ii) a lower level of reaction rate at all potentials. These distinctions were observed over a wide range of temperatures and acid concentrations, but are most evident at elevated temperature in relatively less concentrated  $\text{H}_3\text{PO}_4$ , e.g., 100-150 C, 85-92 percent acid. These are conditions favoring the anodic underpotential deposition process



Damjanovic and co-workers (18) have shown how UPD oxygen "poisons" the oxygen reduction reaction and causes a transition slope to occur as the UPD oxygen coverage increases to more than ca. 10 percent of a monolayer. This self-poisoning effect by UPD oxygen appears to explain the difference in the polarization curves shown in Fig. 7, since it is known that the underpotential deposition of oxygen at elevated temperatures starts at more cathodic potentials on the amorphous clusters of Pt. In fact, independent measurement of the UPD oxygen coverage by cyclic voltammetry indicated the expected transitions in Tafel slopes to be at 0.87 V and 0.52 V on the two different forms of Pt (17). These are exactly the potentials where the transitions were observed.

The activation energy for the reduction of oxygen in acid on the amorphous clusters was lower than that for smooth Pt, implying a stronger interaction with molecular oxygen as well as the previously cited case for water. This implication has been confirmed by recent (7) ESCA studies in our laboratory. The stronger interaction with both water and oxygen leads to a decrease in rate via a compensation effort. This compensation effect was observed previously by Appleby (18) in a study of oxygen reduction in acid on the Group VIII metals, and the effect appears to be operative even for different conformations of Pt. Apparently the stronger interaction of the surface with both water and molecular oxygen (in acid) leads to an unfavorable reaction entropy and to a reduction in the number of active sites.

In alkaline solution, the pattern of observations is similar to those made in acid, but with profoundly different consequences. First, it is interesting to compare the polarization behavior of

standard fuel cell electrodes made from the same Pt catalyst (colloidal Pt on Vulcan XC-72) in acid and alkaline electrolyte, as done in Fig. 8. At 0.8 V potential, the oxygen cathode in  $\text{H}_3\text{PO}_4$  supports a current of  $25 \text{ mA/cm}^2$ , but, in KOH a current of  $900 \text{ mA/cm}^2$  can be supported (!). This dramatically improved catalysis in alkaline electrolyte appears to be due not to a difference in exchange current, but to the difference in Tafel slope. The  $50 \pm 5 \text{ mV}$  Tafel slope observed with this fuel cell electrode has been found in our work to be characteristic of all supported Group VIII metals. An essential difference between acid and alkaline electrolyte is that in acid the carbon support has essentially zero activity for oxygen reduction, while in alkaline solution the support has substantial activity for the two electron reduction of oxygen to peroxide. One might, then, suspect that a kinetic coupling between the metal and the support might exist via a peroxide spillover mechanism. This is easily shown not to be an important sequence for carbon-supported Pt. Polarization curves were obtained using four different catalysts with four different types of carbon black onto which Pt was dispersed: Vulcan XC-72, graphitized Vulcan, acetylene black, and steam-treated acetylene black. The catalysts were individually heat treated to generate the same Pt surface area ( $75 \pm 5 \text{ m}^2/\text{g}$ ) on all supports. Electrodes were also fabricated from the uncatalyzed carbons, and as expected the activity for reduction of oxygen to peroxide varied by orders of magnitude between the least active (graphitized Vulcan) and the most active (Vulcan). However, the Pt-catalyzed carbons produced virtually identical polarization curves in the potential region, 0.8–1.0 V RHE. This result would be expected only if the reduction of oxygen were preferentially at the Pt surface. Since the catalysis with supported Pt is specific to the Pt phase, one can proceed as before to compare the behavior of the amorphous Pt clusters with polycrystalline Pt. Figure 9 is the alkaline electrolyte equivalent of the comparison made in Fig. 7. One can easily see that the comparison yields a similar conclusion, that the cluster catalyst is slightly (factor of 2) less active than polycrystalline Pt in the potential region where both surfaces have significant coverages of UPD oxygen. It seems reasonable to conclude that in alkaline solutions one sees the same type of structure sensitivity as that in acid electrolyte, i.e., stronger interaction with oxygen and water for the highly dispersed amorphous clusters.

The explanation for the dramatic difference in Tafel slope between  $\text{H}_3\text{PO}_4$  and KOH seen in Fig. 8 is not related to either a crystallite size effect nor to a peroxide spillover effect. It is beyond the scope of the present paper to detail the mechanisms that might be proposed. It is the opinion of this investigator that the differences are caused by specific adsorption of anions in  $\text{H}_3\text{PO}_4$  that block the surface for adsorption of oxygen. This blocking reduces the coverage of the surface by adsorbed (UPD) oxygen species to less than 0.1 monolayer, and Langmuir (ideal) adsorption of the

rate-determining intermediate produces the 120 mV slope. The 60 mV Tafel slope in KOH represents a Temkin adsorption condition in the rate-determining step due to the high coverage of the surface by UPD oxygen.

#### 4. Extension to Other Group VIII Metals and Metal Oxides

Because of the potential importance of the peroxide spillover mechanism with carbon-supported catalysts, one must distinguish the properties of supported metal catalysts by the support used. In our experience, the most dramatic effects of the support were seen when transition metal oxides on Vulcan XC-72 are compared to metal oxides on graphitized Vulcan. The oxide clusters were prepared by impregnation of the carbon from soluble chloride or nitrate salts. The cluster size was observed using TEM and found to be in the 30-60 Å regime for both types of carbon support, i.e., the mean cluster size in any one catalyst did not differ by more than a factor of 2 from that in another. Following impregnation, the catalysts were pretreated by heating in air at 300 C for 15 min. ESCA of these catalysts indicated all were converted to oxides as a result of this treatment: Ni, Pd, and Pt to the divalent oxide; Rh to the trivalent oxide; and Ru and Ir to the 4+ oxide. With the exception of Pt and Pd, none could be reduced electrochemically to the metallic state in alkaline solution at 70 C. The polarization behavior for the metals on the Vulcan carbon support lay in a relatively narrow band between the curve for the uncatalyzed carbon support and that for RuO<sub>2</sub>, as depicted in Fig. 10. Within this band, the order of activity was observed to be Ru > Ir ~ Rh ~ Pd ~ Ni. The polarization behavior for the metal oxides supported on graphitized Vulcan was significantly different for all five catalysts in the potential region where the active carbon support is producing substantial quantities of peroxide, e.g., below 0.8 V RHE. The observed Tafel slopes were correspondingly different, having changed from being 55 ± 5 on active carbon to 70 ± 10 mV per decade on graphitized carbon. The ordering in the activity ranking was the same as before but with NiO much less active than the other catalysts. Above 0.85 V RHE, the activity of the different catalysts becomes essentially independent of the chemistry of the carbon support. Kinetic coupling between the carbon support and the metal oxide clusters appeared to maximize in the potential region of 0.7-0.8 V RHE. At lower potentials, diffusion effects predominate and at higher potentials the carbon does not produce sufficient peroxide to cause kinetic coupling.

On a purely practical basis none of the transitional metal oxide cluster catalysts examined here (Ru, Ir, Rh, Pd, Ni) are cost-effective catalysts compared to state-of-the-art carbon-supported Pt catalysts. However, because of the possibility of kinetic coupling between the carbon support and an oxide cluster, an entirely different class of catalysts can be designed to maximize

this effect. Examples of this concept are the spinel oxides of cobalt and nickel and defect manganese dioxide dispersed in activated carbon black. These appear to be the most promising alternatives to the Pt cluster catalysts in certain air electrode applications.

The stability of the spinel oxides of cobalt and nickel is a critical factor in determining the use of these materials in air electrodes. We have observed that the stability of the oxide  $\text{Co}_3\text{O}_4$  increases when the oxide takes on a cluster structure relative to the bulk oxide. This is a consequence of what appears to be a fundamental property of all transition metal oxides: The oxide clusters have a much higher overvoltage for reduction than the bulk oxide. Therefore, metals with passive oxides that undergo reductive dissolution will exhibit stability over a wider potential range when highly dispersed than in bulk form. Since passive oxides of cobalt and manganese break down by reductive dissolution (19), stabilization of the passive oxide by dispersion into clusters would be expected from the fundamental properties of transition metal oxide clusters.

#### Acknowledgements

This work was supported by the Assistant Secretary of Conservation and Renewable Energy, Office of Advanced Conservation Technology, Electrochemical Systems Research Division of the U.S. Department of Energy under contract No. W-7405-ENG-48.

#### References

1. M. Boudart, in Advances in Catalysis, D. Eley, H. Pines, and P. Weisz, eds., Vol. 20, Academic Press, New York (1969), p. 153.
2. R. Burwell et al., J. Catalysis 64, 74 (1980).
3. P. Ross and P. Stonehart, J. Catalysis 48, 42 (1977).
4. H. Kunz and G. Gruver, J. Electrochem. Soc. 122, 1279 (1975).
5. L. Bregoli, Electrochim. Acta 23, 489 (1978); J. Bett et al., Electrochim. Acta 18, 343 (1973); P. Stonehart and J. Lundquist, Electrochim. Acta 18, 907 (1973).
6. P. Ross, in The Electrocatalysis of Fuel Cell Reactions, W. O'Grady, S. Srivivasan, and R. Dudley, eds., The Electrochemical Society, Vol. 79(2) (1979, p. 181.
7. P. Ross, Extended Abstracts, Vol. 79-2, The Electrochemical Society (1979), No.190, to be published in J. Electrochem. Soc. in 1982.
8. C. Adams et al., J. Catalysis 10, 328 (1968).
9. H. Petrow and R. Allen, U.S. Patent 3,492,331, 1976; U.S. Patent 4,044,193, 1977.
10. W. Romanowski, Surf. Sci. 373 (1969).

11. V. Jalan, Extended Abstracts, Vol. 79-2, The Electrochemical Society (1979), No.192.
12. EXAFS Spectroscopy, B. Teo and D. Joy, eds., Plenum, New York, 1981.
13. F. Lytle, personal communication, 1981.
15. K. Kinoshita, J. Lundquist, and P. Stonehart, J. Catalysis 31, 325 (1973).
16. R. Van Hardeveld and F. Hartog, Surf. Sci. 15, 189 (1969).
17. P. Ross, EPRI Report EM-1553, September 1980.
18. A.J. Appleby, Catal. Rev. Sci. Eng. 4, 221 (1970).
19. M. Pourbaix, Atlas of Electrochemical Equilibria in Aqueous Solutions, Pergamon Press, 1966, p. 325.

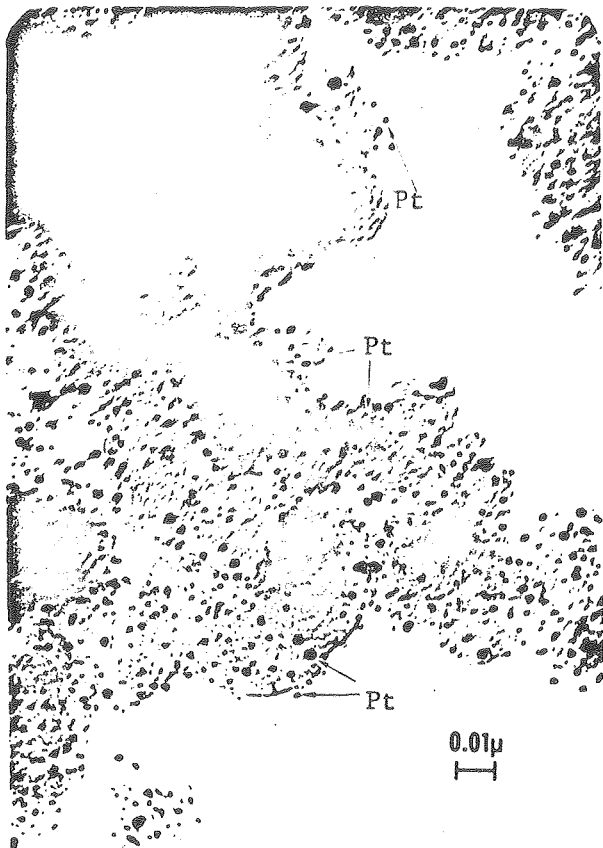
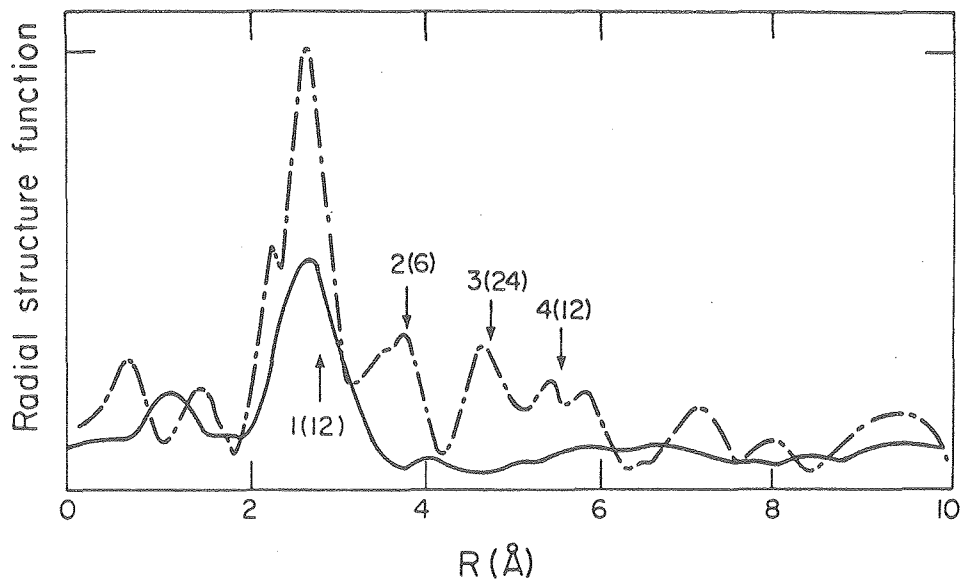


Figure 1. Pt clusters on  
Vulcan XC-72 carbon. 600,000X

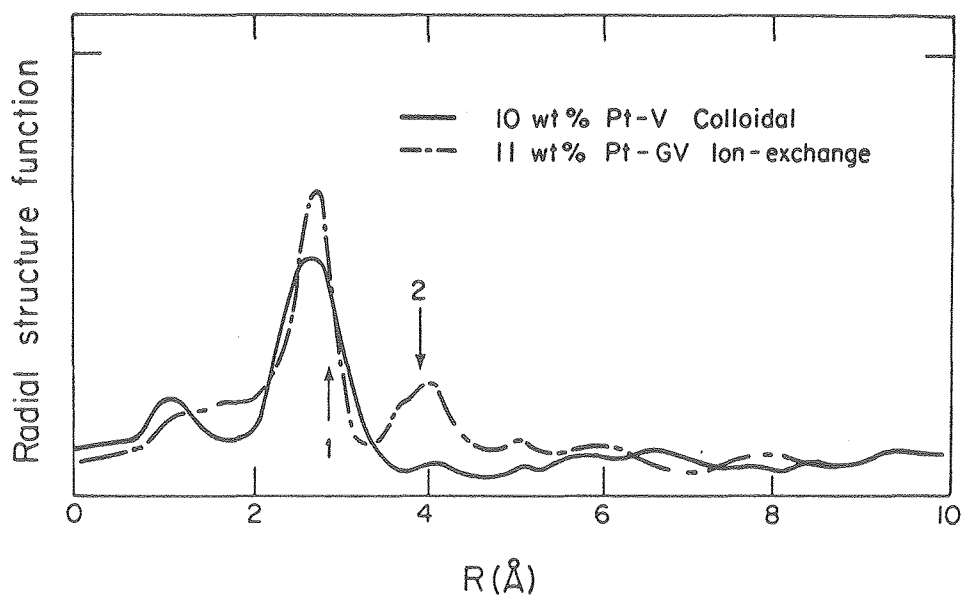
TRANSMISSION ELECTRON MICRO-  
GRAPHS OF Pt CATALYSTS

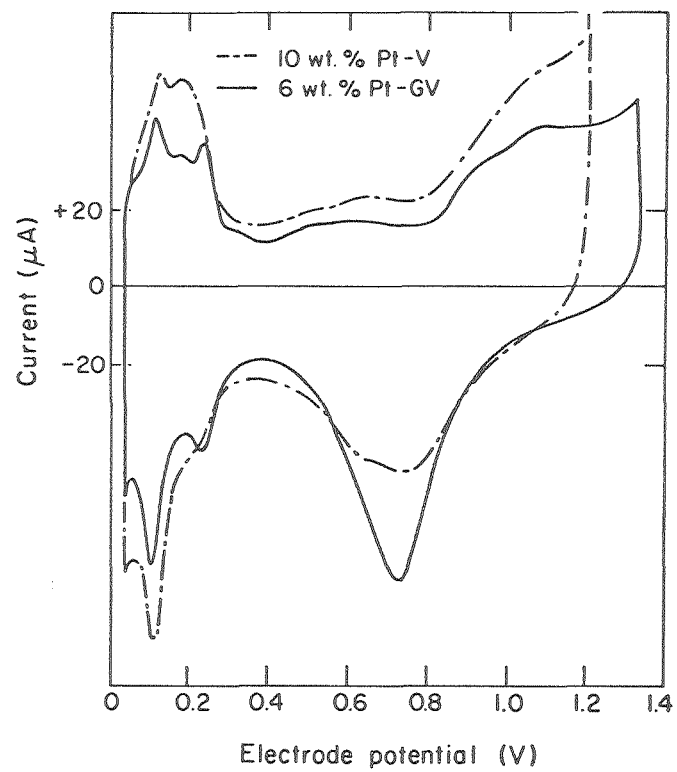
Figure 2. Pt microcrystals on graphitized Vulcan  
XC-72 carbon black. 500,000X



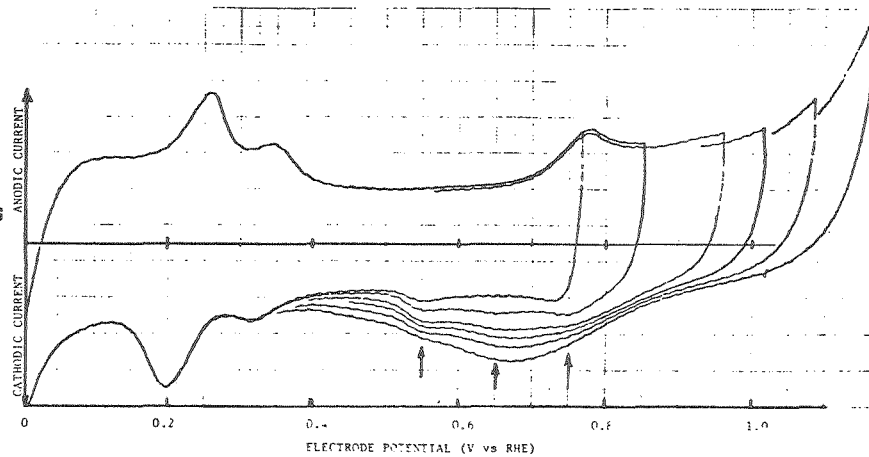
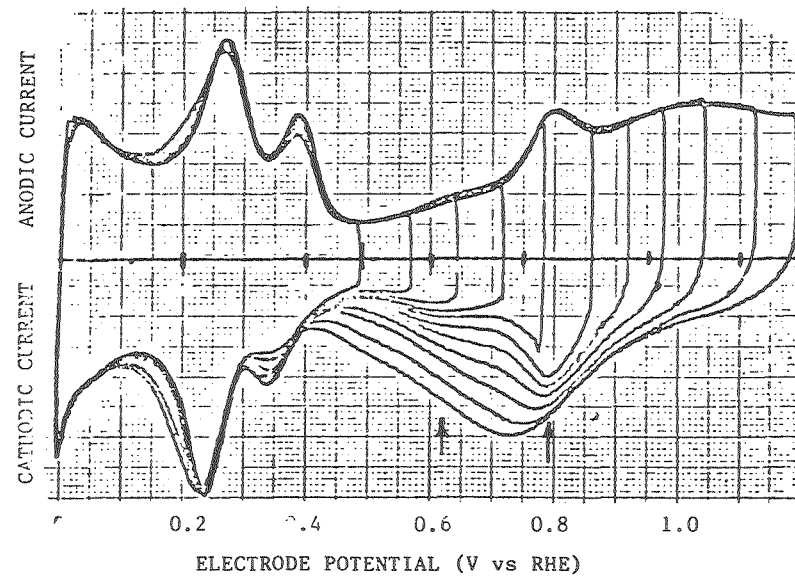


Figures 3&4. Nearest neighbor distributions about a Pt atom in a fcc bulk lattice site (dashed curve) versus a Pt atom in a cluster on Vulcan carbon (solid curve top) and a Pt atom in a cluster on a graphized carbon (dashed curve bottom).





Figures 5 (above) and 6 (right). Cyclic voltammetry curves for supported Pt catalysts in acid (above) and for smooth Pt (upper right) and supported Pt (lower) in alkaline solution.



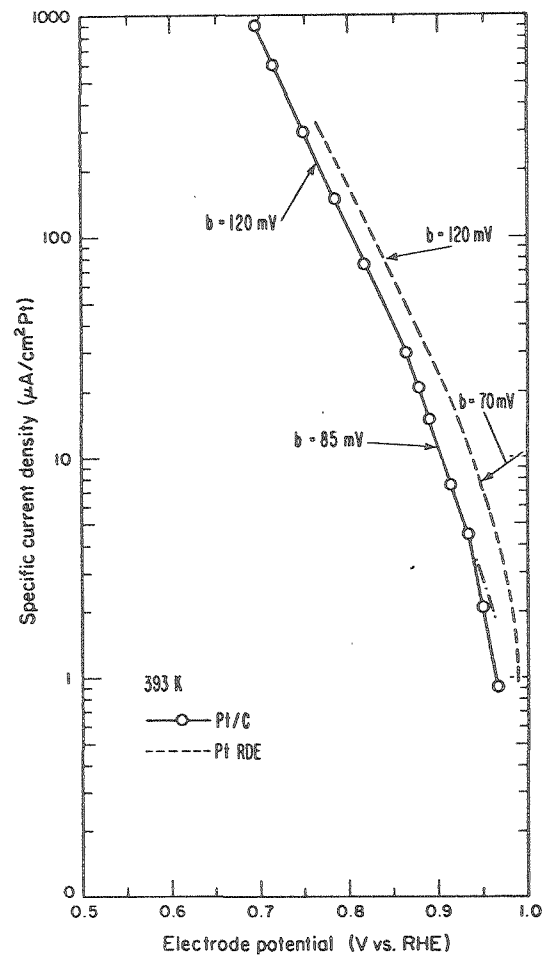


Figure 7. Comparison of the polarization curves for the colloidal Pt on Vulcan carbon catalyst versus a smooth Pt rotating disk electrode. 85%  $\text{H}_3\text{PO}_4$ .

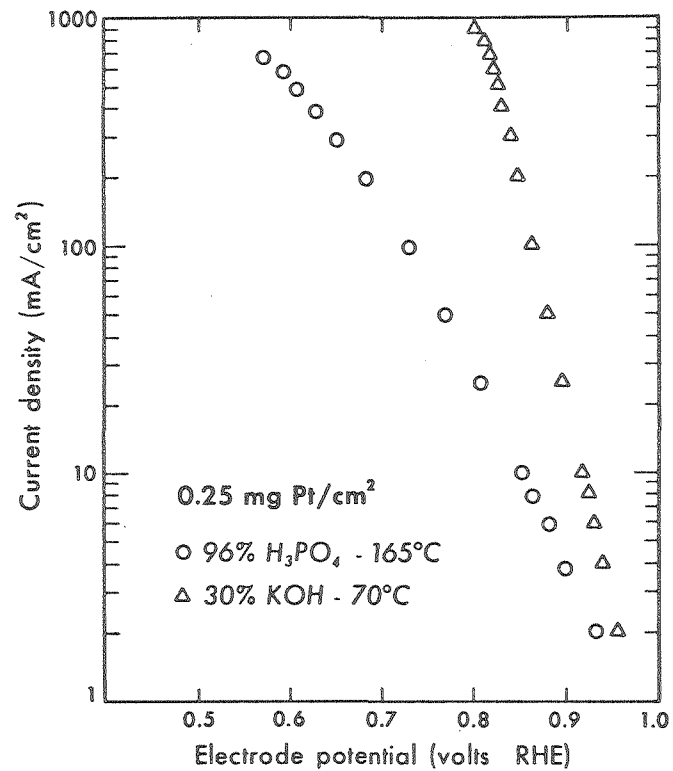


Figure 8. Comparison of the polarization curves for a fuel cell type electrode with colloidal Pt on Vulcan catalyst in acid and alkaline solutions. 1 atm.  $\text{O}_2$ .

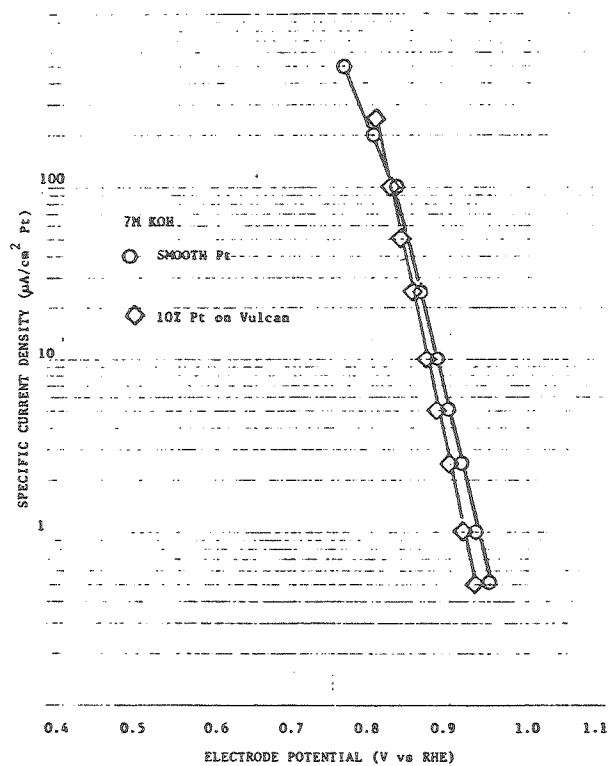


Figure 9. Comparison of the polarization curves for the colloidal Pt on Vulcan carbon catalyst versus a smooth rotating disk electrode. 30% KOH, 25°C.

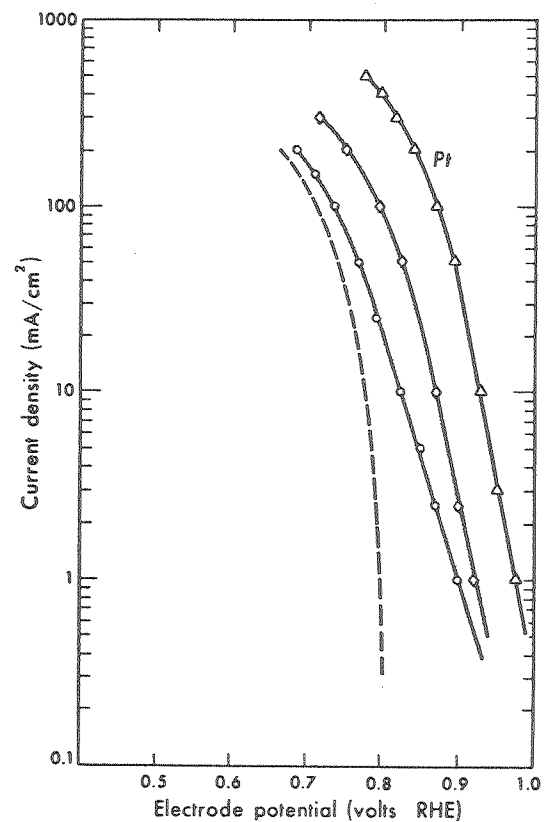


Figure 10. Polarization curves for PTFE-bonded electrodes. Dashed line is uncatalyzed Vulcan carbon. Dark band denotes Vulcan catalyzed by Ru, Pd, Rh, Ir and Ni. 70°C, 23% NaOH.

